

Wurtzite silicon as a potential absorber in photovoltaics: Tailoring the optical absorption by applying strain

C. Rödl,^{1,2,3} T. Sander,^{2,3} F. Bechstedt,^{2,3} J. Vidal,⁴ P. Olsson,^{4,5} S. Laribi,⁴ and J.-F. Guillemoles^{4,6}

¹Laboratoire des Solides Irradiés, Ecole polytechnique, CNRS, CEA-DSM-IRAMIS, Université Paris-Saclay, 91128 Palaiseau cedex, France

²Institut für Festkörperteorie und -optik, Friedrich-Schiller-Universität, Max-Wien-Platz 1, 07743 Jena, Germany

³European Theoretical Spectroscopy Facility (ETSF)

⁴Institute for Research and Development of Photovoltaic Energy (IRDEP), UMR 7174 CNRS / EDF R&D / Chimie ParisTech, 6 quai Watier, 78401 Chatou, France

⁵KTH Royal Institute of Technology, Reactor Physics, Roslagstullsbacken 21, SE-106 91 Stockholm, Sweden

⁶NextPV International Joint Laboratory, CNRS, U. Bordeaux, RCAST, The University of Tokyo, 4-6-1 Komaba, Meguro-ku, Tokyo 153-8904, Japan

(Received 24 January 2014; revised manuscript received 21 June 2015; published 20 July 2015)

We present *ab initio* calculations of the electronic structure and the optical properties of wurtzite Si (Si-IV). We find an indirect band gap of 0.95 eV ($\Gamma_5 \rightarrow M_1$) and an optically forbidden direct gap of 1.63 eV ($\Gamma_5 \rightarrow \Gamma_{10}$), which is due to a backfolding of the L_1 state of Si in the diamond structure (Si-I). Optical absorption spectra including excitonic and local-field effects are calculated. Further, the effects of hydrostatic pressure, uniaxial strain, and biaxial strain on the absorption properties are investigated. Biaxial tensile strains enhance the optical absorption of Si-IV in the spectral range which is relevant for photovoltaic applications. High biaxial tensile strains (>4%) even transform Si-IV into a direct semiconductor.

DOI: [10.1103/PhysRevB.92.045207](https://doi.org/10.1103/PhysRevB.92.045207)

PACS number(s): 71.20.Nr, 78.20.Bh, 71.20.Mq, 71.15.Mb

I. INTRODUCTION

For more than fifty years, Si in the diamond structure (Si-I, space group $Fd\bar{3}m$ or O_h^7), the naturally occurring polymorph, has been one of the most successful active layers in photovoltaic solar cells approaching 75% of its Shockley-Queisser limit [1] efficiency. However, it is obvious that the optical properties of Si are far from being optimal for photovoltaic energy conversion: the indirect band gap [2] results in a low absorption coefficient $\alpha \sim 10^2 \text{ cm}^{-1}$ at the frequencies of interest for photovoltaic devices. Consequently, thick high-quality absorbing layers are needed. Even in high-quality Si, nonradiative processes, such as Auger or Shockley-Read-Hall recombination, prevent further efficiency improvements [3]. Moreover, these requirements in material quality usually translate into the necessity for high-temperature growth and, hence, a cost increase.

Nevertheless, Si is one of the most abundant elements on Earth and its processing can be controlled to an extent never reached for other materials. This asks for exploiting this knowledge in order to achieve improved photovoltaic properties: the direct-to-indirect band gap distance should be reduced to limit the loss of open-circuit voltage, whereas the absorption coefficient should be increased to increase the short-circuit current. A possible route to pursue is to screen the rich phase diagram of Si [4] for polymorphs with more favorable absorption properties. The suitability of some of the semiconducting Si phases for photovoltaics has already been investigated by means of *ab initio* calculations [5–8]. Recently, new semiconducting low-pressure phases of Si with better absorption in the visible spectral range have been predicted theoretically [9]. Si nanoparticles with core structures of high-pressure Si polymorphs have been studied to assess their potential for photovoltaic applications exploiting multiple-exciton generation [10].

Here, we study the optical absorption of the lonsdaleite phase of Si [11], also known as wurtzite Si or Si 2H-4

(Si-IV, space group $P6_3/mmc$ or D_{6h}^4), by means of *ab initio* calculations in order to evaluate its potential as an absorber in photovoltaics. We show that applying strain is a way to tailor its absorption properties very effectively. Si-IV, as a metastable phase, has been stabilized under ambient conditions by laser ablation [12], standard [13], or plasma-enhanced [14] chemical-vapor deposition, nanoindentation [15], or nanoparticle nucleation in gas phase [16,17]. Recently, the existence of the Si-IV phase in nanowires has been questioned [18] but correlated Raman and transmission electron microscopy could show that wurtzite Si is indeed present in Si nanowires [19]. Experimentally, the band gap of Si-IV is unknown, but there are indications for a gap in the order of 1 eV [20], which is promising for photovoltaics.

In the 1970s, the electronic and optical properties of Si-IV were studied by empirical-pseudopotential methods [21,22]. Later, density-functional theory (DFT) was applied to determine the structural parameters and the band gaps in the local-density approximation [23–25]. Here, we employ the more advanced and parameter-free *GW* method [26] of many-body perturbation theory to calculate quasiparticle (QP) band structures and band gaps. Subsequently, optical absorption spectra are computed in the independent-quasiparticle approximation (IQPA) and solving the Bethe-Salpeter equation (BSE) to include excitonic and local-field effects [27]. These calculations allow one to identify the key features of the band structure that are responsible for the absorption onset and the location of the indirect band gap. Moreover, we apply hydrostatic pressure, uniaxial, and biaxial strain to the atomic structure of Si-IV in order to investigate the variation of the band gap and the optical absorption under these constraints. This allows us to identify the most promising distortions for enhancing the potential of Si-IV as a photovoltaic absorber.

The paper is organized as follows. In Sec. II, we give a brief summary of the computational details. In Sec. III, the band gap and optical absorption of Si-IV in the equilibrium

structure are computed and analyzed in terms of transitions. Section IV focuses on the impact of various types of strain on the electronic and optical properties. Finally, in Sec. V, a summary is given and conclusions are drawn.

II. COMPUTATIONAL DETAILS

All DFT and *GW* calculations have been performed using VASP [28–30] with the projector-augmented wave method which yields an accuracy comparable to all-electron calculations. The Si 3*s* and 3*p* electrons are treated as valence electrons. The wave functions outside the augmentation spheres are expanded in plane waves up to a cutoff energy of 450 eV. For the Brillouin-zone (BZ) integrations, $10 \times 10 \times 10$ (Si-I) or $10 \times 10 \times 5$ **k** points (Si-IV) have been used.

Structural relaxations have been carried out using the AM05 exchange-correlation functional [31], which yields a lattice constant of 5.437 Å for Si-I in excellent agreement with the experimental value of 5.431 Å [32]. To obtain the equilibrium structure, atomic coordinates have been relaxed for a series of volumes until all forces were below 1 meV/Å. The resulting energy-volume curve was fitted to the Murnaghan equation of state [33] to identify the energy-minimizing configuration.

QP band structures in the *GW* approximation have been calculated perturbatively in the G_0W_0 one-shot approach on top of the AM05 electronic structure. The electronic screening has been computed at 200 frequency grid points including 150 (Si-I) or 300 bands (Si-IV) in the sum over states. Reciprocal lattice vectors up to a plane-wave cutoff of 200 eV were included in the inversion of the dielectric matrix to take local-field effects into account. The QP corrections were calculated separately for each strained structure. For Si-I, we obtain excellent agreement with experiment for the indirect gap $E_g^{\text{ind}} = 1.14$ eV (experiment 1.17 eV [2]). The direct gap of Si-I is $E_g^{\text{dir}} = 3.20$ eV (experiment 3.40 eV [34]) within this approach.

Optical absorption spectra for the various strained structures of Si-IV have been calculated in the IQPA using a grid

of $24 \times 24 \times 12$ shifted **k** points. Usually, the δ functions that occur in the imaginary part of the dielectric function $\varepsilon(\omega)$ (see, e.g., Ref. [27]) are represented by Lorentzians with a broadening of the order of 0.1 eV which ensures a smoothing of the absorption curves. However, this broadening is significantly larger than the inverse lifetimes at the absorption onset. To avoid these far-reaching Lorentzian tails within the QP gap, we represent the δ function by a smooth nascent δ function with compact support, the bump function, which is given by $B_b(\omega) = 1/(cb) \exp[b^2/(\omega^2 - b^2)]$ for $|\omega| < b$ and $B_b(\omega) = 0$ elsewhere. The width parameter b is adjusted such that the height of the curve corresponds to the height of the normalized Lorentzian and c is a normalization constant.

The imaginary part of the dielectric function has also been calculated solving the BSE. The static screening of the electron-hole interaction in the BSE Hamiltonian is described by an analytic function [35] that depends on the electronic static dielectric constant ε_∞ and the average charge density. The eigenvalue problem of the electron-hole Hamiltonian is solved by means of a time-evolution scheme [36]. For the BSE spectra, the BZ was sampled with $24 \times 24 \times 24$ (Si-I) or $24 \times 24 \times 12$ shifted **k** points (Si-IV). Phonon-assisted indirect optical transitions are not included in our approach.

III. OPTICAL ABSORPTION OF SI-IV IN ITS EQUILIBRIUM STRUCTURE

A. Absorption spectrum

Structural relaxation yields the lattice parameters $a = 3.828$ Å, $c = 6.325$ Å, $c/a = 1.652$, $u = 0.374$ for Si-IV (see Table I) in excellent agreement with the experimental findings [20] $a = 3.837$ Å, $c = 6.317 \pm 0.012$ Å, and $c/a = 1.646 \pm 0.008$. The c/a ratio and the internal cell parameter u are close to the values $c/a = \sqrt{8/3}$ and $u = 3/8$ for the ideal wurtzite structure. The band gap $E_g^{\text{ind}} = 0.95$ eV is indirect and occurs between the Γ_5 and the M_1 state (see Fig. 1, nomenclature as in Refs. [22,37]). This value is in excellent

TABLE I. Lattice parameters and QP band gaps for strained Si-IV. Strain is given in terms of relative change in volume (hydrostatic pressure), c (uniaxial strain), or a lattice constant (biaxial strain).

Strain		-5%	-4%	-3%	-2%	-1%	+0%	+1%	+2%	+3%	+4%	+5%
Hydrostatic pressure	a (Å)	3.763	3.776	3.789	3.802	3.815	3.828	3.841	3.854	3.867	3.880	3.893
	c (Å)	6.225	6.244	6.265	6.285	6.305	6.325	6.345	6.366	6.386	6.407	6.427
	u	0.374	0.374	0.374	0.374	0.374	0.374	0.374	0.374	0.374	0.374	0.374
	E_g^{ind} (eV)	0.85	0.87	0.89	0.91	0.94	0.95	0.97	0.99	1.01	1.03	1.04
	E_g^{dir} (eV)	1.79	1.76	1.73	1.70	1.67	1.63	1.60	1.57	1.54	1.51	1.48
Uniaxial strain	a (Å)	3.861	3.854	3.847	3.841	3.834	3.828	3.822	3.816	3.811	3.806	3.801
	c (Å)	6.008	6.072	6.135	6.198	6.261	6.325	6.388	6.451	6.514	6.578	6.641
	u	0.384	0.381	0.379	0.377	0.376	0.374	0.373	0.371	0.370	0.369	0.368
	E_g^{ind} (eV)	0.52	0.69	0.79	0.85	0.90	0.95	1.00	1.05	1.09	1.03	0.96
	E_g^{dir} (eV)	0.92	1.16	1.31	1.43	1.53	1.63	1.73	1.82	1.91	1.99	1.90
Biaxial strain	a (Å)	3.637	3.675	3.714	3.752	3.790	3.828	3.867	3.905	3.943	3.982	4.020
	c (Å)	6.462	6.430	6.401	6.373	6.348	6.325	6.303	6.284	6.264	6.249	6.234
	u	0.363	0.366	0.368	0.370	0.372	0.374	0.376	0.378	0.379	0.381	0.382
	E_g^{ind} (eV)	0.68	0.83	0.95	0.96	0.96	0.95	0.94	0.93	0.90	0.87	0.67
	E_g^{dir} (eV)	1.74	1.99	2.17	2.00	1.82	1.63	1.45	1.26	1.07	0.89	0.67

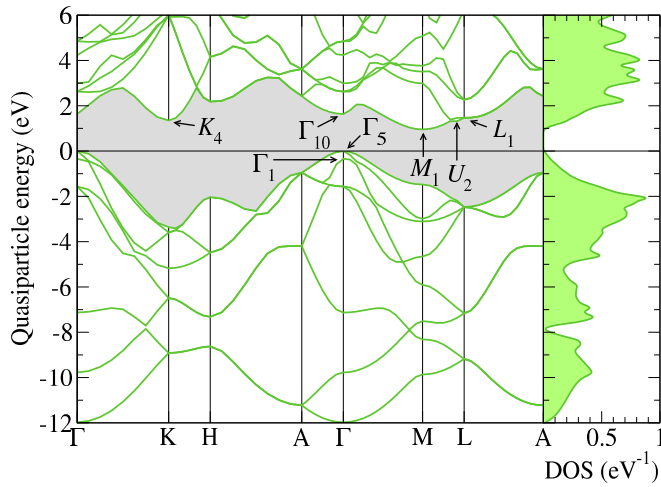


FIG. 1. (Color online) Quasiparticle band structure and density of states (DOS) per atom for Si-IV. Relevant high-symmetry states in the vicinity of the band gap are labeled. The nomenclature follows Refs. [22,37]. The valence-band maximum is set to zero.

agreement with a previous calculation [6]. The smallest direct gap $E_g^{\text{dir}} = 1.63$ eV between Γ_5 and Γ_{10} is due to a backfolding of the L_1 state of Si-I.

In Fig. 2, the imaginary part of the macroscopic dielectric function of Si-IV is shown in the IQPA and solving the BSE for both polarization directions. Strong excitonic effects, i.e., the electron-hole interaction, enhance the low-energy part of the spectrum by a redistribution of spectral weight. The total width of the absorption spectrum resembles the width of the spectrum of Si-I, which is shown for comparison in Fig. 2. Differences are observable for the peak structure (due to different van-Hove singularities) and at the absorption onset. Moreover, we observe a strong polarization dependence with an enhanced absorption in the range of $\sim 2.5 \dots 3.5$ eV for extraordinary

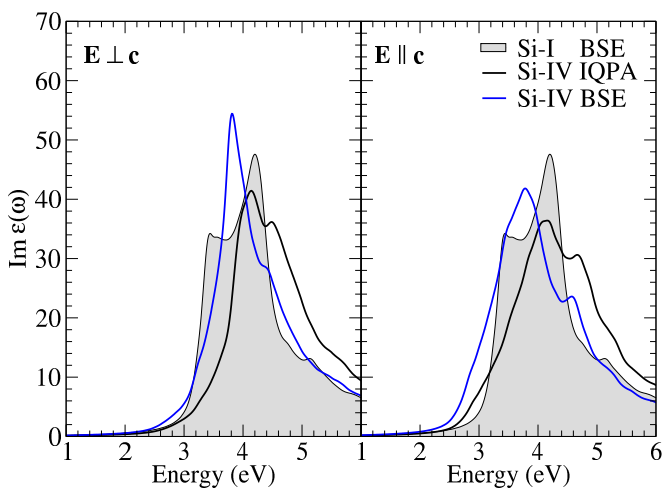


FIG. 2. (Color online) Imaginary part of the dielectric function $\varepsilon(\omega)$ of Si-IV calculated in the IQPA and including excitonic and local-field effects (BSE). Spectra are plotted for ordinary ($\mathbf{E} \perp \mathbf{c}$) and extraordinary polarization ($\mathbf{E} \parallel \mathbf{c}$). The imaginary part of the dielectric function of Si-I including excitonic and local-field effects is shown for comparison.

polarization with respect to ordinary polarization. Consistently with the much smaller direct gap of Si-IV, the absorption edge is found at lower energies compared to Si-I. The absorption of Si-IV exceeds the absorption of Si-I in the whole visible spectral range, in particular, for extraordinary polarization. However, the absorption remains weak directly above the band gap and significant spectral weight can be observed only above ~ 2.5 eV.

B. Analysis in terms of transitions

The absorption properties above the onset can be understood by investigating the dominant optical interband transitions (see Fig. 3). In terms of their energies, only transitions from the three highest valence bands into the three lowest conduction bands around Γ and along the U line between Γ and M can potentially contribute to the absorption at energies right above the band gap [second panel of Fig. 3(a)]. However, the optical matrix elements for transitions between the three highest valence bands and the first conduction band are vanishingly small in the relevant part of the BZ

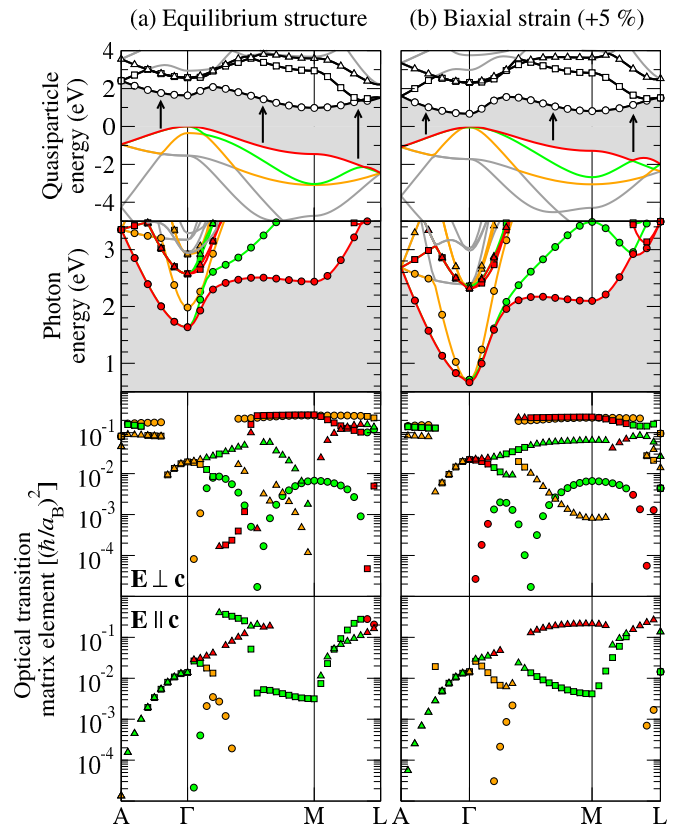


FIG. 3. (Color online) Illustration of the optical transitions that govern the absorption onset of Si-IV in the equilibrium structure (a) and for +5% of biaxial strain (b). First panel: QP band structures. Second panel: joint band structures for the optical transition energies. Third and fourth panel: oscillator strengths of the optical transitions for both polarizations. Transitions from the three highest valence bands (red, green, orange in the top panel) into the three lowest conduction bands (empty circles, squares, and triangles in the top panel) are represented by combining the respective colors and symbols in the lower panels.

(note the logarithmic scale), which is a consequence of the backfolding of indirect $\Gamma \rightarrow L$ transitions in Si-I to direct $\Gamma \rightarrow \Gamma$ transitions in Si-IV. Also the transitions along the Γ - M line, where the highest valence band and lowest conduction band are almost parallel, which leads to a high joint density of states, are dipole forbidden and do not contribute to the absorption.

The absorption above ~ 2.5 eV results from transitions between the three highest valence bands and the second and third conduction band. The strong rise in absorption above 3 eV is due to the backfolding of the $L_3' \rightarrow L_1$ transition in Si-I to the $\Gamma_6 \rightarrow \Gamma_{10}$ transition in Si-IV (fourth and fifth valence band to first conduction band). Also the polarization dependence of the spectra is evident from Fig. 3 reflecting the anisotropy of the atomic structure of Si-IV: transitions between the highest valence bands and the second and third conduction bands along the Γ - A line are forbidden for ordinary but allowed for extraordinary polarization.

IV. OPTICAL ABSORPTION OF STRAINED Si-IV

A. Definitions and relations

The enhancement of optical absorption in Si-IV compared to Si-I in the spectral range relevant for photovoltaics can be improved by applying strain to the system. Here, we investigate the impact of compressive and tensile strains on the absorption properties of Si-IV.

For small crystal strains ε_j , the associated stresses σ_i follow Hooke's law, which reads

$$\sigma_i = \sum_{j=1}^6 C_{ij} \varepsilon_j \quad (1)$$

in Voigt notation. Here, $\boldsymbol{\varepsilon} = (\varepsilon_{xx}, \varepsilon_{yy}, \varepsilon_{zz}, \varepsilon_{yz}, \varepsilon_{zx}, \varepsilon_{xy})$ is the vector of the six independent components of the symmetric strain tensor. The components of the stress tensor $\boldsymbol{\sigma}$ are defined analogously. For crystals with lonsdaleite (or wurtzite [38]) symmetry, the nonzero components of the symmetric elasticity tensor are $C_{11} = C_{22}$, C_{33} , C_{12} , $C_{13} = C_{23}$, $C_{44} = C_{55}$, and $C_{66} = \frac{1}{2}(C_{11} - C_{12})$ [39].

Here, we investigate hydrostatic pressure, uniaxial strain along the c axis, and biaxial strain in the plane perpendicular to the c axis. None of these lattice distortions breaks the symmetry of the D_{6h}^4 space group. All shear strains and stresses are zero. Consequently, Hooke's law reduces to

$$\sigma_{xx} = \sigma_{yy} = (C_{11} + C_{12}) \varepsilon_{xx} + C_{13} \varepsilon_{zz}, \quad (2a)$$

$$\sigma_{zz} = 2C_{13} \varepsilon_{xx} + C_{33} \varepsilon_{zz} \quad (2b)$$

with the normal strains

$$\varepsilon_{xx} = \varepsilon_{yy} = \frac{a - a_{\text{eq}}}{a_{\text{eq}}} \quad \text{and} \quad \varepsilon_{zz} = \frac{c - c_{\text{eq}}}{c_{\text{eq}}}, \quad (3)$$

where a_{eq} and c_{eq} are the lattice constants of the equilibrium structure and a and c the lattice constants of the strained crystal.

In the case of hydrostatic pressure, the normal stresses are equal and given by the (negative) pressure, $\sigma_{xx} = \sigma_{yy} = \sigma_{zz} = -p$. Using Eq. (2), this leads to the relation

$$\varepsilon_{zz} = \frac{C_{11} + C_{12} - 2C_{13}}{C_{33} - C_{13}} \varepsilon_{xx} \quad (4)$$

between the strains along and perpendicular to the c direction. With $dV/V = 2\varepsilon_{xx} + \varepsilon_{zz}$ for small volume changes dV/V around the equilibrium volume, the isothermal bulk modulus $B_0 = -V \frac{dp}{dV} \Big|_{p=0}$ can be written as

$$B_0 = \frac{(C_{11} + C_{12})C_{33} - 2C_{13}^2}{(C_{11} + C_{12}) - 4C_{13} + 2C_{33}}. \quad (5)$$

Hydrostatic pressure is simulated by fixing the volume of the unit cell and relaxing the a and the c lattice constants as well as all internal coordinates.

For uniaxial strain along the c axis, the normal stress is nonzero, $\sigma_{zz} \neq 0$, and the in-plane stress components vanish, $\sigma_{xx} = \sigma_{yy} = 0$. Under these conditions, the out-of-plane and in-plane strains are linked by

$$\varepsilon_{zz} = -\frac{C_{11} + C_{12}}{C_{13}} \varepsilon_{xx}, \quad (6)$$

which follows again directly from Eq. (2). These relations immediately allow one to determine the Poisson ratio $\nu = -\varepsilon_{xx}/\varepsilon_{zz} = C_{13}/(C_{11} + C_{12})$ and the Young modulus $E = \sigma_{zz}/\varepsilon_{zz} = C_{33} - 2C_{13}^2/(C_{11} + C_{12})$ of the material. To model uniaxial strain, constrained relaxations with fixed c lattice constants have been performed for a series of volumes. The respective constrained equilibrium structures have been obtained by a fit to the Murnaghan equation of state.

Biaxial strain perpendicular to the c axis is described by $\sigma_{zz} = 0$ and $\sigma_{xx} = \sigma_{yy} \neq 0$. From Eq. (2), the relation

$$\varepsilon_{zz} = -\frac{2C_{13}}{C_{33}} \varepsilon_{xx} \quad (7)$$

for the out-of-plane and in-plane strains can be obtained. The biaxial relaxation coefficient reads $R^B = -\varepsilon_{zz}/\varepsilon_{xx} = 2C_{13}/C_{33}$ and the biaxial modulus $Y = \sigma_{xx}/\varepsilon_{xx} = (C_{11} + C_{12}) - 2C_{13}^2/C_{33}$. Note in particular, that tensile (compressive) uniaxial strain along the c axis and compressive (tensile) biaxial strain perpendicular to the c axis do not represent identical situations. Biaxial strain is simulated by constrained relaxations with fixed a lattice constant for a series of volumes, followed by a fit to the Murnaghan equation of state to determine the constrained equilibrium structure.

B. Structural and elastic properties

Experimentally, deviations from the equilibrium lattice constants of up to 6% have been realized [13], which is why we study changes of volume dV/V (hydrostatic pressure) and lattice constants dc/c (uniaxial strain) and da/a (biaxial strain) in a range from -5 to $+5\%$. The lattice parameters of the strained structures are compiled in Table I. The linear relation between the change in the lattice constants and the applied strain as given by Eqs. (4), (6), and (7) (i.e., Hooke's law) holds in good approximation throughout the entire range of investigated distortions. Only the internal cell parameter u exhibits significant nonlinear behavior in the cases of uniaxial and biaxial strain.

Fitting the energy-volume dependence for hydrostatic pressure to the Murnaghan equation of state yields the isothermal bulk modulus of Si-IV, $B_0 = 92.8$ GPa, and its pressure derivative $B' = 4.24$. Exploiting the relations derived in Sec. IV A, we obtain the Poisson ratio $\nu = 0.1567$, the Young modulus

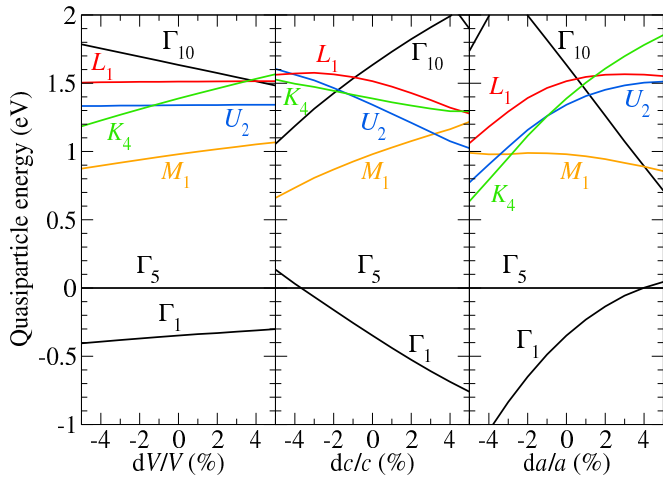


FIG. 4. (Color online) Evolution of selected high-symmetry QP states of Si-IV with hydrostatic pressure, uniaxial, and biaxial strain. The nomenclature follows Refs. [22,37]. For convenience, the corresponding states are marked in the band structure in Fig. 1. The variation of all states is plotted with respect to the Γ_5 state whose energy is set to zero for all strains.

$E = 202$ GPa, the biaxial relaxation coefficient $R^B = 0.3478$, and the biaxial modulus $Y = 224$ GPa. The corresponding elastic stiffness constants read $C_{11} + C_{12} = 237$ GPa, $C_{13} = 37$ GPa, and $C_{33} = 213$ GPa.

C. Band gap

The evolution of the high-symmetry states close to the band gap in dependence on the applied strain is shown in Fig. 4. The resulting values for the lowest indirect and direct band gaps are summarized in Table I. Figure 4 illustrates that the behavior of electronic states with different symmetry depends strongly on the nature of the constraints applied to the atomic structure.

For hydrostatic pressure, the observed effects are small over the whole range of investigated volume changes (pressures). With increasing volume, the direct band gap of Si-IV shrinks, a behavior similar to semiconductors with a direct allowed sp gap.

In the case of uniaxial strain, the indirect and direct band gaps decrease with decreasing c lattice constants. The lowest indirect gap moves to the $\Gamma_1 \rightarrow M_1$ transition for strains of -4% and below, whereas it goes to the $\Gamma_5 \rightarrow U_2$ transition for tensile strains of 4% and above. The $\Gamma_1 \rightarrow \Gamma_{10}$ transition becomes the lowest direct gap for compressive strains of 4% and more (see Fig. 4).

Applying tensile biaxial strains causes a dramatic reduction of the direct gap which, eventually, leads to a direct semiconductor with a $\Gamma_1 \rightarrow \Gamma_{10}$ gap for tensile strains larger than 4% . For compressive strains, on the contrary, the direct gap increases and the indirect gap moves to $\Gamma_5 \rightarrow K_4$ for strains of -3% and below (see Fig. 4).

D. Absorption spectra

The calculation of absorption spectra using the BSE is computationally very demanding. For this reason, we first

calculate the absorption spectra of all strained structures in the IQPA to identify the strained structure with the highest absorption in the visible spectral range. In a second step, the optical absorption of the most promising strained structure is computed using the BSE and compared to the absorption of the Si-IV equilibrium structure. The inclusion of excitonic effects leads to a redistribution of spectral weight to lower energies and will, hence, only further increase the optical absorption close to the band gap.

Since we focus on the absorption close to the onset, the use of the standard Lorentzian broadening of ~ 0.1 eV is inappropriate. This broadening is significantly larger than the inverse lifetimes at the absorption onset and leads to spurious far-reaching tails inside the band gap that entirely disguise the absorption onset, in particular when absorption coefficients are plotted. Instead of Lorentzians, we use smooth nascent δ functions with compact support here (see Sec. II). This implies that the absorption within the band gap rapidly drops to zero. Phononic contributions to the absorption are disregarded here in order to give a clear idea about the electronic transitions and their evolution under crystal strain.

The optical absorption coefficients calculated for the strained structures in the IQPA are shown in Fig. 5. As can be expected from the small changes in the electronic structure, hydrostatic pressure has little impact on the absorption properties. Applying pressure, i.e., decreasing the volume, increases the direct band gap and lowers the optical absorption at the onset. Moreover, the indirect band gap becomes smaller. Thus, applying hydrostatic pressure to Si-IV deteriorates its potential as photovoltaic absorber.

Uniaxial tensile strains of 4% or more modify the absorption onset qualitatively. This is due to the $\Gamma_5 \rightarrow \Gamma_8$ transition which becomes the lowest direct transition and leads to an additional absorption peak. In the equilibrium structure, the Γ_8 state is associated to the fourth conduction band. Si-IV under compressive uniaxial strains exhibits qualitatively the same absorption characteristics as the equilibrium structure, but with a considerably lower absorption onset that shifts down to 0.9 eV for 5% of uniaxial compressive strain. The absorption is significantly larger for ordinary polarization [see Fig. 5(b)]. Even though compressive uniaxial strains could improve the electronic properties of Si-IV with regard to photovoltaic applications, these conditions are experimentally hard to realize.

Also for large compressive biaxial strains, the $\Gamma_5 \rightarrow \Gamma_8$ transition is energetically lower than the $\Gamma_5 \rightarrow \Gamma_{10}$ transition yielding an additional absorption peak at the onset [see Fig. 5(c)]. Tensile biaxial strains, on the other hand, redshift the absorption edge of Si-IV to lower energies (0.7 eV for $+5\%$ of biaxial strain), with an absorption that is significantly stronger for ordinary polarization. For $+4\%$ of strain, the indirect $\Gamma_5/\Gamma_1 \rightarrow M_1$ and the direct $\Gamma_5/\Gamma_1 \rightarrow \Gamma_{10}$ gaps are almost equal in size and with 0.9 eV close to the maximum of the Shockley-Queisser efficiency-limit curve. As it can be seen from Fig. 3(b), the increased absorption for the biaxially strained structure is mainly due to the smaller band gaps and not to changes of the optical transition matrix elements.

Among the studied structural distortions, we consider tensile biaxial strains as the most promising distortions that

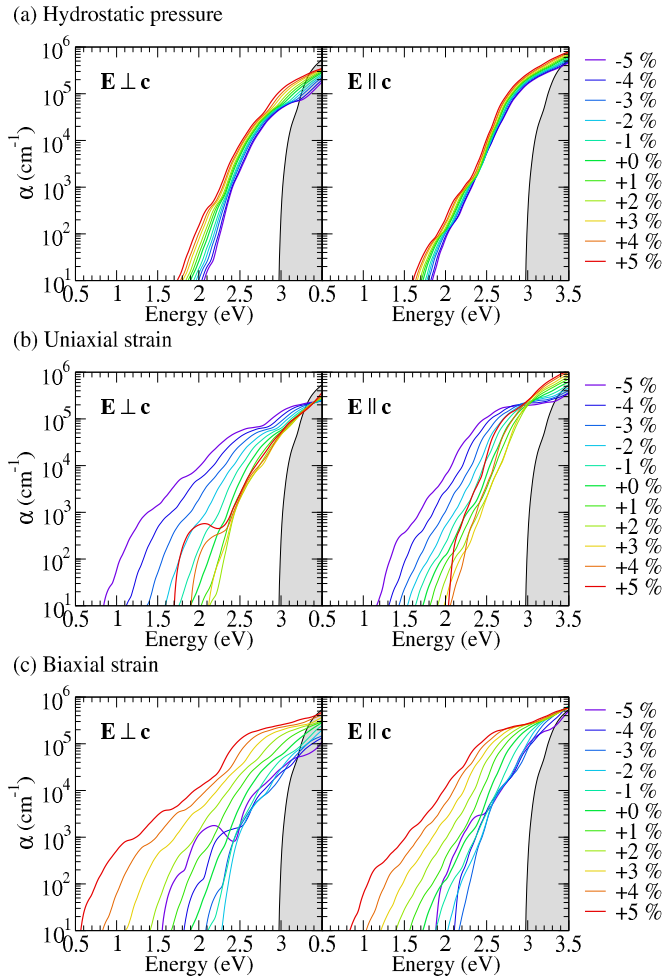


FIG. 5. (Color online) Absorption coefficient $\alpha(\omega)$ of strained Si-IV in the IQPA for ordinary ($\mathbf{E} \perp \mathbf{c}$) and extraordinary ($\mathbf{E} \parallel \mathbf{c}$) polarization. Strains are given in percents for the relative changes of dV/V (hydrostatic pressure), dc/c (uniaxial strain), and da/a (biaxial strain). For comparison, the absorption coefficient of Si-I is shown as shaded area.

can lead to an improvement of the photovoltaic properties of Si-IV, namely a shrinkage of the indirect-to-direct band-gap distance in combination with an increase of the absorption coefficient in the visible spectral range. In Fig. 6, the optical absorption including excitonic and local-field effects is shown for Si-I, Si-IV in its equilibrium structure, and Si-IV under +5% of biaxial strain. Compared to the IQPA calculation, the inclusion of the electron-hole interaction via the BSE further increases the optical absorption in the low-energy region. It leads to an enhancement of oscillator strength close to the gap. From Fig. 6, it is evident that the optical absorption of biaxially strained Si-IV has a much bigger overlap with the solar reference spectrum than the absorption of unstrained Si-IV. This holds for both polarization directions.

V. SUMMARY AND CONCLUSIONS

In summary, we have used state-of-the-art methods of many-body perturbation theory to determine the electronic

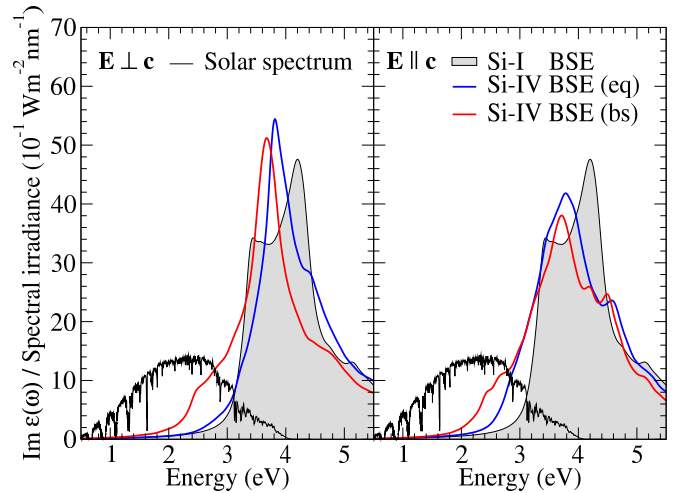


FIG. 6. (Color online) Imaginary part of the dielectric function $\varepsilon(\omega)$ of Si-IV including excitonic and local-field effects (BSE). The absorption of Si-IV is shown for the equilibrium structure (eq) and for 5% of tensile biaxial strain (bs). Spectra are plotted for ordinary ($\mathbf{E} \perp \mathbf{c}$) and extraordinary polarization ($\mathbf{E} \parallel \mathbf{c}$). The imaginary part of the dielectric function of Si-I including excitonic and local-field effects and the solar spectral irradiance [40] are shown for comparison.

structure and optical absorption spectrum of Si-IV including quasiparticle, excitonic, and local-field effects. The impact of hydrostatic pressure, uniaxial, and biaxial strain on the band gap and the optical absorption has been investigated. Large biaxial tensile strains turn Si-IV into a direct-gap semiconductor with a gap of 0.7–0.9 eV. Among the investigated distortions, tensile biaxial strain constitutes the most promising structural deformation for achieving a significantly enhanced optical absorption in the visible spectral range with respect to Si-IV in the equilibrium geometry.

Tailoring the band gap and the optical absorption onset by structural distortions opens the way to utilize strained Si-IV as active layer in photovoltaic devices with absorption properties that are more favorable than those of both Si-IV in its equilibrium geometry or Si-I. The strained geometries may be realized by growing layered heterostructures of Si-IV along the c direction in alternation with another material that constrains the a lattice constant. Nanostructuring constitutes another possibility to impose the lattice constraints. The high absorption in the strained structure could enable thin-film solar cells (below 10 μm) that approach the radiative limit [1] for this material.

ACKNOWLEDGMENTS

Financial support from the FFW Austria within the framework of the SFB 25 IR-ON, the European Research Council (ERC GA No. 320971), and the European Commission within the framework of the ETSF (GA No. 211956) is gratefully acknowledged. This work started as ETSF user project No. 372. C.R. thanks the European Commission Marie Curie Actions for financial support within the framework of the CEA Eurotalents program and GENCI (Project 544) for computing time.

- [1] W. Shockley and H. J. Queisser, *J. Appl. Phys.* **32**, 510 (1961).
- [2] W. Bludau, A. Onton, and W. Heinke, *J. Appl. Phys.* **45**, 1846 (1974).
- [3] A. Richter, F. Werner, A. Cuevas, J. Schmidt, and S. W. Glunz, *Energy Procedia* **27**, 88 (2012).
- [4] J. Crain, G. J. Ackland, and S. J. Clark, *Rep. Prog. Phys.* **58**, 705 (1995).
- [5] Y. Fujimoto, T. Koretsune, S. Saito, T. Miyake, and A. Oshiyama, *New J. Phys.* **10**, 083001 (2008).
- [6] B. D. Malone, J. D. Sau, and M. L. Cohen, *Phys. Rev. B* **78**, 035210 (2008).
- [7] B. D. Malone, J. D. Sau, and M. L. Cohen, *Phys. Rev. B* **78**, 161202 (2008).
- [8] B. D. Malone, S. G. Louie, and M. L. Cohen, *Phys. Rev. B* **81**, 115201 (2010).
- [9] S. Botti, J. A. Flores-Livas, M. Amsler, S. Goedecker, and M. A. L. Marques, *Phys. Rev. B* **86**, 121204 (2012).
- [10] S. Wippermann, M. Vörös, D. Rocca, A. Gali, G. Zimanyi, and G. Galli, *Phys. Rev. Lett.* **110**, 046804 (2013).
- [11] R. H. Wentorf, Jr., and J. S. Kasper, *Science* **139**, 338 (1963).
- [12] Y. Zhang, Z. Iqbal, S. Vijayalakshmi, and H. Grebel, *Appl. Phys. Lett.* **75**, 2758 (1999).
- [13] A. Fontcuberta i Morral, J. Arbiol, J. Prades, A. Cirera, and J. Morante, *Adv. Mater.* **19**, 1347 (2007).
- [14] P.-J. Alet, L. Yu, G. Patriarche, S. Palacin, and P. Roca i Cabarrocas, *J. Mater. Chem.* **18**, 5187 (2008).
- [15] S. Minomura and H. G. Drickamer, *J. Phys. Chem. Solids* **23**, 451 (1962).
- [16] V. Domnich, Y. Gogotsi, and S. Dub, *Appl. Phys. Lett.* **76**, 2214 (2000).
- [17] G. Viera, M. Mikikian, E. Bertran, P. Roca i Cabarrocas, and L. Boufendi, *J. Appl. Phys.* **92**, 4684 (2002).
- [18] C. Cayron, M. Den Hertog, L. Latu-Romain, C. Mouchet, C. Secouard, J.-L. Rouviere, E. Rouviere, and J.-P. Simonato, *J. Appl. Crystallogr.* **42**, 242 (2009).
- [19] F. J. Lopez, E. R. Hemesath, and L. J. Lauhon, *Nano Lett.* **9**, 2774 (2009).
- [20] J. M. Besson, E. H. Mokhtari, J. Gonzalez, and G. Weill, *Phys. Rev. Lett.* **59**, 473 (1987).
- [21] J. D. Joannopoulos and M. L. Cohen, *Phys. Rev. B* **7**, 2644 (1973).
- [22] J. D. Joannopoulos and M. L. Cohen, *Phys. Rev. B* **8**, 2733 (1973).
- [23] C.-Y. Yeh, Z. W. Lu, S. Froyen, and A. Zunger, *Phys. Rev. B* **46**, 10086 (1992).
- [24] M. Murayama and T. Nakayama, *Phys. Rev. B* **49**, 4710 (1994).
- [25] C. Raffy, J. Furthmüller, and F. Bechstedt, *Phys. Rev. B* **66**, 075201 (2002).
- [26] L. Hedin, *Phys. Rev.* **139**, A796 (1965).
- [27] G. Onida, L. Reining, and A. Rubio, *Rev. Mod. Phys.* **74**, 601 (2002).
- [28] G. Kresse and J. Furthmüller, *Comput. Mater. Sci.* **6**, 15 (1996).
- [29] G. Kresse and D. Joubert, *Phys. Rev. B* **59**, 1758 (1999).
- [30] M. Shishkin and G. Kresse, *Phys. Rev. B* **74**, 035101 (2006).
- [31] R. Armiento and A. E. Mattsson, *Phys. Rev. B* **72**, 085108 (2005).
- [32] W. Parrish, *Acta Crystallogr.* **13**, 838 (1960).
- [33] F. D. Murnaghan, *Proc. Natl. Acad. Sci. USA* **30**, 244 (1944).
- [34] R. R. L. Zucca and Y. R. Shen, *Phys. Rev. B* **1**, 2668 (1970).
- [35] F. Bechstedt, R. Del Sole, G. Cappellini, and L. Reining, *Solid State Commun.* **84**, 765 (1992).
- [36] W. G. Schmidt, S. Glutsch, P. H. Hahn, and F. Bechstedt, *Phys. Rev. B* **67**, 085307 (2003).
- [37] J. Zak, A. Casher, M. Glück, and Y. Gur, *The Irreducible Representations of Space Groups*, edited by J. Zak (W. A. Benjamin, New York, 1969).
- [38] J.-M. Wagner and F. Bechstedt, *Phys. Rev. B* **66**, 115202 (2002).
- [39] C. Giovazzo, H. L. Monaco, G. Artioli, D. Viterbo, G. Ferraris, G. Gilli, G. Zanotti, and M. Catti, *Fundamentals of Crystallography*, 2nd ed. (Oxford University Press, New York, 2002).
- [40] ASTM G173-03(2012), *Standard Tables for Reference Solar Spectral Irradiances: Direct Normal and Hemispherical on 37° Tilted Surface*, ASTM International (West Conshohocken, PA, USA, 2012).